

## Resistivity in the vicinity of a van Hove singularity

Barber, Mark E.; Gibbs, Alexandra S.; Maeno, Yoshiteru; Mackenzie, Andrew P.; Hicks, Clifford W.

DOI:

[10.1103/PhysRevLett.120.076602](https://doi.org/10.1103/PhysRevLett.120.076602)

License:

None: All rights reserved

*Document Version*

Peer reviewed version

*Citation for published version (Harvard):*

Barber, ME, Gibbs, AS, Maeno, Y, Mackenzie, AP & Hicks, CW 2018, 'Resistivity in the vicinity of a van Hove singularity: Sr<sub>2</sub>RuO<sub>4</sub> under uniaxial pressure', *Physical Review Letters*, vol. 120, no. 7, 076602.  
<https://doi.org/10.1103/PhysRevLett.120.076602>

[Link to publication on Research at Birmingham portal](#)

### General rights

Unless a licence is specified above, all rights (including copyright and moral rights) in this document are retained by the authors and/or the copyright holders. The express permission of the copyright holder must be obtained for any use of this material other than for purposes permitted by law.

- Users may freely distribute the URL that is used to identify this publication.
- Users may download and/or print one copy of the publication from the University of Birmingham research portal for the purpose of private study or non-commercial research.
- User may use extracts from the document in line with the concept of 'fair dealing' under the Copyright, Designs and Patents Act 1988 (?)
- Users may not further distribute the material nor use it for the purposes of commercial gain.

Where a licence is displayed above, please note the terms and conditions of the licence govern your use of this document.

When citing, please reference the published version.

### Take down policy

While the University of Birmingham exercises care and attention in making items available there are rare occasions when an item has been uploaded in error or has been deemed to be commercially or otherwise sensitive.

If you believe that this is the case for this document, please contact [UBIRA@lists.bham.ac.uk](mailto:UBIRA@lists.bham.ac.uk) providing details and we will remove access to the work immediately and investigate.

# Resistivity in the Vicinity of a Van Hove Singularity: $\text{Sr}_2\text{RuO}_4$ Under Uniaxial Pressure

M. E. Barber,<sup>1,2,\*</sup> A. S. Gibbs,<sup>1,†</sup> Y. Maeno,<sup>3</sup> A. P. Mackenzie,<sup>1,2,‡</sup> and C. W. Hicks<sup>2,§</sup>

<sup>1</sup>*Scottish Universities Physics Alliance, School of Physics and Astronomy,  
University of St. Andrews, St. Andrews KY16 9SS, U.K.*

<sup>2</sup>*Max Planck Institute for Chemical Physics of Solids, Nöthnitzer Str. 40, 01187 Dresden, Germany*

<sup>3</sup>*Department of Physics, Graduate School of Science, Kyoto University, Kyoto 606-8502, Japan*

(Dated: September 20, 2017)

We report the results of a combined study of the normal state resistivity and superconducting transition temperature  $T_c$  of the unconventional superconductor  $\text{Sr}_2\text{RuO}_4$  under uniaxial pressure. There is strong evidence that as well as driving  $T_c$  through a maximum at  $\sim 3.5$  K, compressive strains  $\varepsilon$  of nearly 1 % along the crystallographic [100] axis drive the  $\gamma$  Fermi surface sheet through a Van Hove singularity, changing the temperature dependence of the resistivity from  $T^2$  above and below the transition region to  $T^{1.5}$  within it. This occurs in extremely pure single crystals in which the impurity contribution to the resistivity is  $< 100$  n $\Omega$  cm, so our study also highlights the potential of uniaxial pressure as a more general probe of this class of physics in clean systems.

When the shape or filling of a Fermi surface is changed such that it changes either the way that it connects in momentum ( $k$ ) space or disappears altogether, its host metal is said to have undergone a Lifshitz transition [1]. This zero temperature transition has no associated local Landau order parameter, and is in fact one of the first identified examples in condensed matter physics of a topological transition. Lifshitz transitions usually involve traversing Van Hove singularities (VHS). These are points or, in the presence of interactions, regions of  $k$ -space associated in two-dimensional systems with divergences in the density of states [2]. Lifshitz transitions are therefore often associated with formation or strengthening of ordered states, with superconductivity [3–6] and magnetism [7, 8] among the most prominently studied examples. They are also expected, even in the absence of order, to affect the electrical transport [4, 9, 10].

Although of considerable interest theoretically, experimentally tuning materials to Lifshitz transitions is challenging. In zero applied magnetic field it usually requires non-stoichiometric doping to change the band filling. In practice, this introduces disorder, which always complicates the understanding of the observed behaviour. Magnetic field enables clean tuning by changing band energies for opposite spins through the Zeeman term, and has been used to good effect in the study of a number of systems [11–16]. However, unless the intrinsic bandwidths are already very small, large fields are required to reach Lifshitz transitions, and magnetic fields also couple either constructively or destructively to many forms of order.

Although high hydrostatic pressure is an option [19], it needs to be strong enough either to change the relative band filling in multi-band materials or to substantially change the shape of a Fermi surface. As we illustrate in Fig. 1, uniaxial pressure is in principle better suited to changing the shape of Fermi surfaces without the need to change the carrier number. For a single band Fermi surface in two dimensions, the shape change introduced by

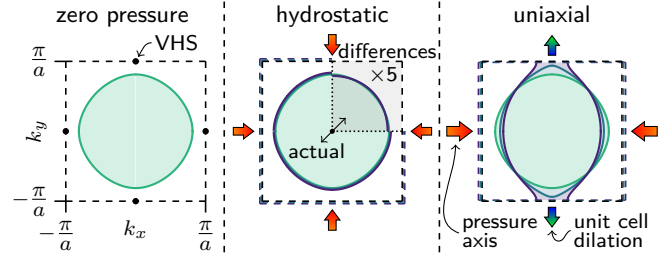


FIG. 1. (color online). An illustrative single band tight-binding model depicting the changes of a two-dimensional Fermi surface under different forms of pressure. In general, hydrostatic pressure increases the relative weight of the next-nearest neighbour hopping term causing the Fermi surface to become slightly more circular [17]. Under equal uniaxial pressures much larger distortions occur changing the Fermi surface from a closed to an open orbit by traversing the VHS. Simulation parameters are given in [18].

applying hydrostatic pressure is negligible, while similar levels of uniaxial pressure introduce a large distortion. Uniaxial pressure is therefore particularly well suited to tuning to the class of Lifshitz transition involving a topological change from a closed to an open Fermi surface by traversing the VHS associated with saddle points along one direction of  $k$  space. It was used a long time ago in experiments tensioning single crystal whiskers of the three-dimensional superconductors aluminium [20] and cadmium [21] but traversing the transition had only a weak effect;  $T_c$ , for example, changed by only  $\sim 20$  mK.

Recently, we have developed novel methods of applying high levels of uniaxial pressure to single crystals that are not restricted to whiskers and are well suited to studying the more interesting case of materials with quasi-2D electronic structure [22, 23]. In a multi-band metal, it is possible for one of the Fermi surface sheets of a pressured crystal to undergo a large shape change while others are affected much less strongly. As shown by the modelled Fermi surfaces in Fig. 2(a), this is the case for the

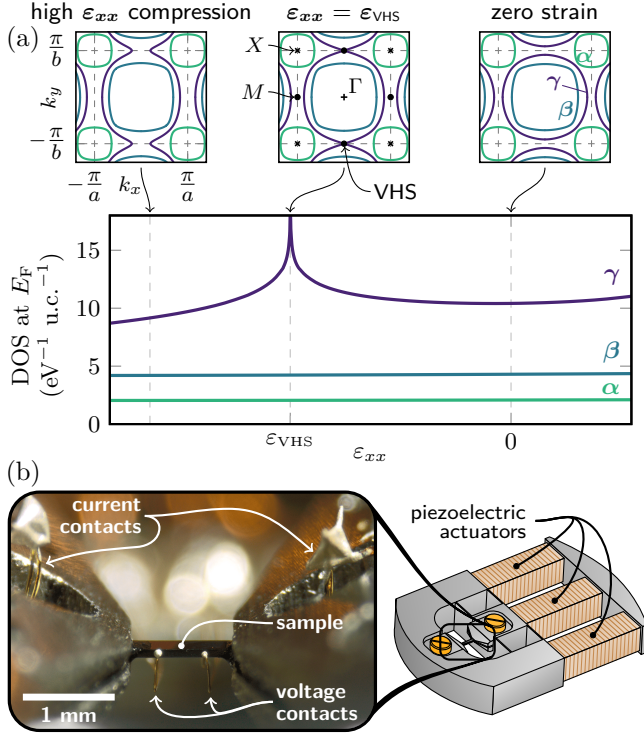


FIG. 2. (color online). (a)  $\text{Sr}_2\text{RuO}_4$  Fermi surface and density of states at the Fermi level as a function of applied anisotropic strain, calculated using a tight-binding model derived from the experimentally determined Fermi surface at ambient pressure [31] after introducing the simplest strain dependence for the hopping terms. See [18] for further simulation details. Fermi surfaces at three representative compressions highlight the Lifshitz transition as the  $\gamma$ -band reaches the VHS. (b) A sample mounted for resistivity measurements under uniaxial pressure and a schematic of the piezoelectric-based device used for generating the pressure.

quasi-2D material studied in this paper,  $\text{Sr}_2\text{RuO}_4$  [24–28], which is predicted by first-principles calculations to undergo a Lifshitz transition when the lattice is compressed by  $\sim 0.75\%$  along a  $\langle 100 \rangle$  lattice direction [29]. In previous work on this material we have shown that the superconducting transition temperature  $T_c$  rises from its unstrained value of 1.5 K and peaks strongly at  $\sim 3.5$  K at a compressive strain of  $\approx 0.6\%$  [29]. While it is tempting to associate this with the occurrence of a Lifshitz transition, measurements reported to date were based only on the study of the diamagnetic susceptibility, and did not in themselves constitute proof that such a transition had occurred. For example, the peak could also correspond to a transition into a magnetically ordered state induced around the Lifshitz transition [30]. To further investigate both the existence of a Lifshitz transition and its consequences, we report here simultaneous magnetic susceptibility and electrical resistivity measurements on single crystals of  $\text{Sr}_2\text{RuO}_4$  under  $\langle 100 \rangle$  compressive strains of up to 1%, and temperatures between 1.2 and 40 K.

A schematic of our experimental apparatus and a pho-

tograph of a crystal mounted for resistivity measurements are shown in Fig. 2(b). The resistivity  $\rho_{xx}$  is measured in the same direction as the applied pressure. Simultaneous measurements of magnetic susceptibility were performed using a detachable drive and pickup coil on a probe that could be moved into place directly above the sample without disturbing the contacts for the resistivity measurements. We rely exclusively on the susceptibility measurements to determine  $T_c$ , to avoid being deceived by percolating, higher- $T_c$  current paths. Resistivity and susceptibility were measured using standard a.c. meth-

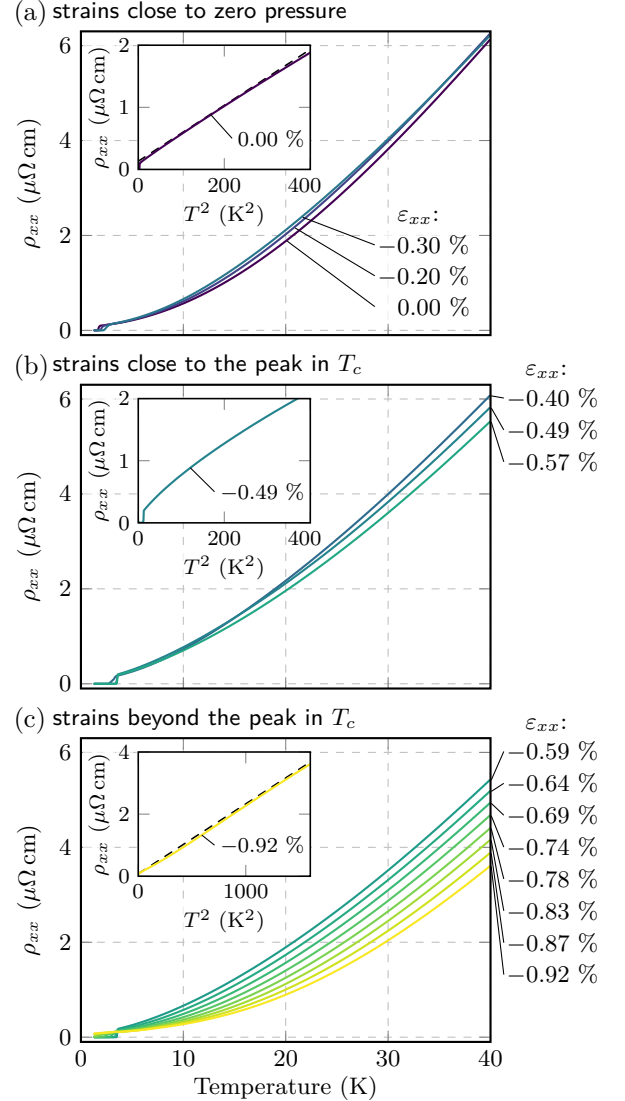


FIG. 3. (color online). Temperature dependence of the resistivity  $\rho_{xx}$  at a variety of  $[100]$  compressive strains: (a) low strains where quadratic temperature dependence is still observed below  $\sim 20$  K, (b) strains close to the peak in  $T_c$  where the strongest deviations from  $T^2$  resistivity are observed, and (c) the highest strains measured showing the larger extent of the  $T^2$  region of resistivity and the rapid strain dependence of its weight.

ods at drive frequencies between 50–500 Hz and 0.1–10 kHz respectively, in a  $^4\text{He}$  cryostat in which cooling was achieved via coupling to a helium pot that could be pumped to reach its base temperature of 1.2 K. Uniaxial pressure was applied by appropriate high voltage actuation of the piezo stacks shown in Fig. 2(b), using procedures described in Refs. [22, 23, 29, 32, 33]. After some slipping of the sample mounting epoxy during initial compression, all resistivity data repeated though multiple strain cycles, indicating that the sample remained within its elastic limit. Two samples were studied to ensure reproducibility; further details are given in [18].

In Fig. 3 we show  $\rho_{xx}(T)$  at various applied compressions. Consistent with the high  $T_c$  of 1.5 K at zero strain, the residual resistivity  $\rho_{\text{res}}$  is less than 100 n $\Omega$  cm, corresponding to an impurity mean free path  $\ell$  in excess of 1  $\mu\text{m}$  [34]. The well-established  $\rho_{\text{res}} + AT^2$  dependence [35, 36] is seen below  $\sim 20$  K in the unstrained sample (Fig. 3(a) and inset). As the strain  $\varepsilon_{xx}$  increases to 0.2 % the quadratic temperature dependence is retained but  $A$  increases, qualitatively consistent with the increase in density of states expected on the approach to a Van Hove singularity. Further increase of the strain results in the resistivity reaching a maximum and deviating significantly from a quadratic temperature dependence, as shown both in the main plot of Fig. 3(b) and in the inset. As the strain is increased further, the drop in  $T_c$  is accompanied by a fall of the resistivity, simultaneous with a recovery of the  $\rho_{\text{res}} + AT^2$  form and a drop of the  $A$  coefficient. By  $\varepsilon_{xx} = -0.92$  %  $T_c$  has fallen to below 1.2 K, the resistivity remains almost perfectly quadratic to over 30 K, and  $A$  has dropped to  $\sim 40$  % of its value in the unstrained material (Fig. 3(c) and inset).

As noted above, one mechanism by which the peak in  $T_c$  might not correspond to the Van Hove singularity is if it is cut off by a different order promoted by proximity to the Van Hove singularity. This is the prediction of the functional renormalization group calculations on uniaxially pressurized  $\text{Sr}_2\text{RuO}_4$  of Ref. [30], which predict formation of spin density wave order. However, the data shown in Fig. 3 give no evidence for any instability other than superconductivity across the range of pressures studied. There is no indication of any transition in any of the  $\rho_{xx}(T)$  curves, before or after the peak in  $T_c$ . Also,  $\rho_{xx}$  falls on the other side of the peak, whereas especially at low temperature the opening of a magnetic gap should generally cause resistivity to increase.

To correlate features of the resistivity with the evolution of the superconductivity more precisely, we plot, in Fig. 4, two key quantities associated with the resistivity and show how they compare with the strain dependence of  $T_c$ . In Fig. 4(a) we show a logarithmic derivative plot that gives an indication of the strain-dependent power  $\delta$  associated with a postulated  $\rho_{\text{res}} + BT^\delta$  temperature dependence. Constructing such a plot involves assumptions [18] but it gives a first indication of the behaviour of

the resistivity and shows that  $\delta$  drops from 2 at low and high strains to  $\sim 1.5$  at  $\varepsilon_{xx} = -0.5$  %. In Fig. 4(b) we plot the results of a measurement of the resistivity measured under continuous strain tuning at 4.5 K (chosen to be 1 K higher than the maximum  $T_c$ , to be free of any influence of superconductivity).  $\rho_{xx}$  is also maximum at  $\varepsilon_{xx} \approx -0.5$  %. In Fig. 4(c) we plot  $T_c$  and  $\rho_{xx}(T = 4.5 \text{ K})$

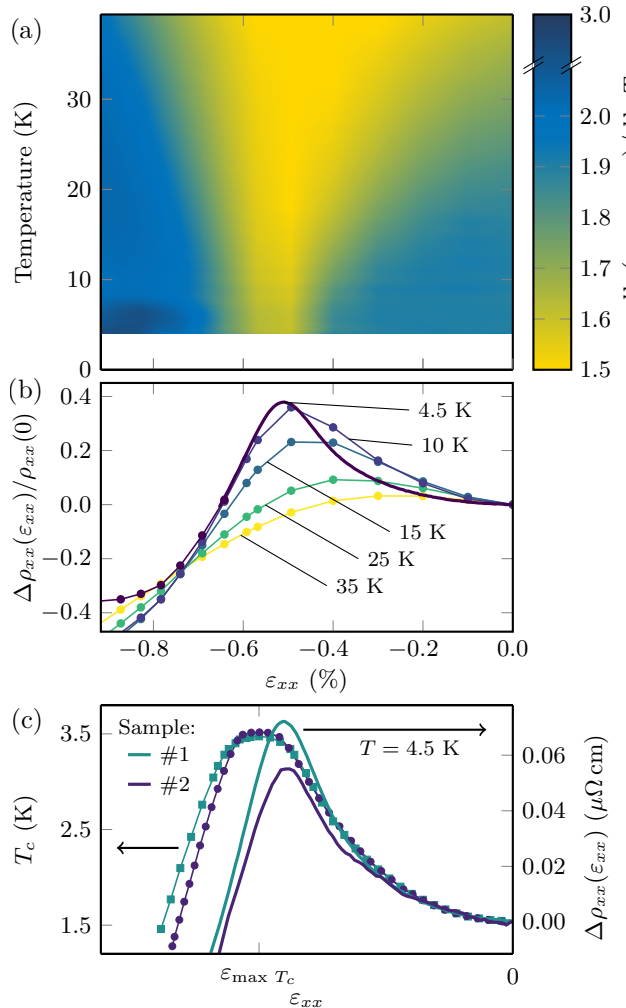


FIG. 4. (color online). (a) Resistivity temperature exponent  $\delta$  plotted against temperature and strain.  $\rho_{\text{res}}$  was first extracted from fits of the type  $\rho = \rho_{\text{res}} + BT^\delta$  and then  $\delta$  was calculated as a function of temperature by  $d \ln(\rho - \rho_{\text{res}}) / d \ln T$  [18]. (b) Elastoresistance at various temperatures. Values were calculated by interpolating between separate temperature ramps at a series of constant strains (Fig. 3), except for 4.5 K where the strain was swept continuously up to  $\varepsilon_{xx} \approx 0.7$  %. (c) Comparison of the strain dependence of  $T_c$  measured by magnetic susceptibility and the resistivity enhancement under continuous strain tuning at 4.5 K. Two samples are shown with  $\rho_{\text{res}}$  of 80 and 20 n $\Omega$  cm in which  $\rho_{xx}$  rises to 190 and 95 n $\Omega$  cm respectively at 4.5 K. In panel (c) the strain scales have been normalised to the peak in  $T_c$ .  $\varepsilon_{xx}$  at the peak in  $T_c$  is  $-0.56$  % and  $-0.59$  % for samples 1 and 2, respectively, and this difference is within our error for determining sample strain.



against  $\varepsilon_{xx}$  for this sample and for a second sample with a slightly lower residual resistivity. The magnitude of the resistivity increase is approximately the same for both samples, and for both the resistivity peaks at a slightly lower compression than  $T_c$ .

Taken together, we believe that the data shown in Figs. 3 and 4 give strong evidence that we have successfully traversed the VHS in  $\text{Sr}_2\text{RuO}_4$  by applying uniaxial pressure. This is not the first time that this VHS has been reached by some form of tuning; in fact it has previously been traversed in the  $(\text{Sr},\text{Ba},\text{La})_2\text{RuO}_4$  system by explicit chemical doping of  $\text{La}^{3+}$  onto the Sr site [37, 38] and by using epitaxial thin film techniques to grow biaxially strained stoichiometric  $\text{Sr}_2\text{RuO}_4$  and  $\text{Ba}_2\text{RuO}_4$  thin films [17]. In both cases, a drop of resistive exponent  $\delta$  to approximately 1.4 was reported [17, 37]. The novelty of our results is that they are observed in crystals with such low levels of disorder. In the previous experiments on the ruthenates, the inelastic component of the resistivity has been approximately the same magnitude by 30 K as the residual resistivity [17, 37], while here it is a factor of forty larger. Combined with the facts that the data shown in Figs. 3 and 4 cover a full decade of temperature above the maximum  $T_c$ , and that the Fermi surface of  $\text{Sr}_2\text{RuO}_4$  is well known, we believe that this means that our results can set an experimental benchmark for testing theoretical understanding of the evolution of transport properties around an externally tuned Lifshitz transition. A full treatment of the problem will require further theoretical work that is beyond the scope of this paper, but we close with a discussion of what is known so far and the extent to which it applies to our results.

The effect on resistivity of traversing a Van Hove singularity has been studied in idealized single band models, taking into account the energy dependence of the density of states, electron-electron Umklapp processes and impurity scattering. Depending on the form postulated for the density of states, variational calculations using Boltzmann transport theory in the relaxation time approximation have discussed resistivities of the form  $\rho(T) = \rho_{\text{res}} + bT^2 \ln(c/T)$  or  $\rho(T) = \rho_{\text{res}} + bT^{3/2}$  [9]. Within experimental uncertainties, these two possibilities cannot be distinguished, see Fig. 5. Numerical calculations going beyond the relaxation time approximation [39, 40] predict  $\delta < 2$ . The amount by which  $\delta$  is reduced depends on the degree of nesting of the Fermi surface;  $\delta = 1$  is predicted for perfect nesting.

It is interesting to note that tuning to a VHS is evidently not sufficient to obtain the  $T$ -linear resistivity that is often associated with quantum criticality. Although the resistivity is enhanced in the vicinity of the VHS,  $\rho(T)$  does not increase at nearly the rate seen for systems with  $T$ -linear resistivity [41].

Although the calculated temperature dependences fit the data well, we caution that it is questionable whether

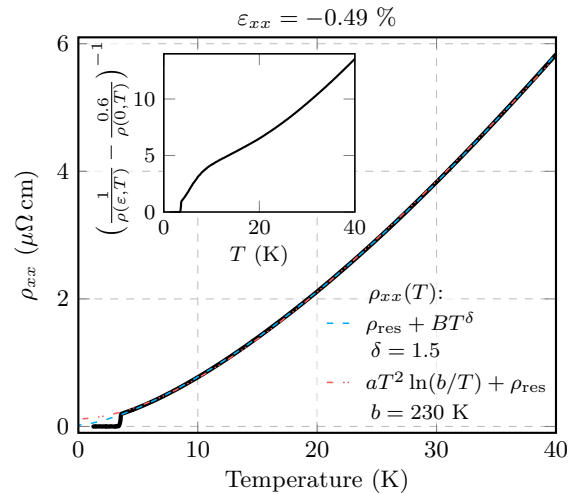


FIG. 5. (color online). A comparison of different fitting functions for the temperature dependence of the resistivity at  $\varepsilon_{xx} = -0.49\%$ . Both fits are made between 4 K and 40 K. The inset shows the same resistivity curve after subtracting 60 % of the zero strain conductivity, estimated to be the contribution of the  $\gamma$  band if the scattering rate of the  $\alpha$  and  $\beta$  sheet carriers is unaffected by the traversal of the Lifshitz point on the  $\gamma$  sheet.

they are even applicable to  $\text{Sr}_2\text{RuO}_4$ . As illustrated in Fig. 2(a), it is not a single-band, but a three-band metal, and both the tight-binding calculation presented here and full first-principles calculations [29] show that the Lifshitz transition occurs on the  $\gamma$  Fermi surface sheet. In contrast, the  $\alpha$  and  $\beta$  sheets show almost no distortion at these strains. At zero strain the average Fermi velocities of each sheet are known, so for a sheet-independent scattering rate it is straightforward to estimate that the  $\alpha$  and  $\beta$  sheets contribute over 60 % of the conductivity. Under the postulate that the scattering rate of the  $\alpha$  and  $\beta$  sheet carriers is unaffected by the traversal of the Lifshitz point on the  $\gamma$  sheet, the contribution of the  $\gamma$  sheet to the resistivity at  $-0.49\%$  strain is shown in the inset to Fig. 5, and seen to be qualitatively very different from any single-band prediction. The likely implication of this analysis is that the scattering rate changes induced by the change in shape of the  $\gamma$  sheet affect both the  $\alpha$  and  $\beta$  sheet carriers just as strongly as those on the  $\gamma$  sheet. However, it seems far from obvious that this should automatically be the case, and it would be very interesting to see full multi-band calculations for  $\text{Sr}_2\text{RuO}_4$  to assess the extent to which it can be understood using conventional theories of metallic transport.

In conclusion, we believe that the results that we have presented in this paper represent an experimental benchmark for the effects on resistivity of undergoing a Lifshitz transition against a background of very weak disorder. Our results stimulate further theoretical work on this topic, and highlight the suitability of uniaxial stress for probing this class of physics.

We thank J. Schmalian, E. Berg, and M. Sigrist for useful discussions and H. Takatsu for sample growth. We acknowledge the support of the Max Planck Society and the UK Engineering and Physical Sciences Research Council under grants EP/I031014/1 and EP/G03673X/1. Y.M. acknowledges the support by the Japan Society for the Promotion of Science Grants-in-Aid for Scientific Research (KAKENHI) JP15H05852 and JP15K21717.

---

\* barber@cpfs.mpg.de

† Present address: ISIS Facility, Rutherford Appleton Laboratory, Chilton, Didcot OX11 0QX, U.K.

‡ andy.mackenzie@cpfs.mpg.de

§ hicks@cpfs.mpg.de

- [1] I. M. Lifshitz, Zh. Eksp. Teor. Fiz. **38**, 1569 (1960), [Sov. Phys. JETP **11**, 1130 (1960)].
- [2] G. E. Volovik, Low Temp. Phys. **43**, 47 (2017).
- [3] C. C. Tsuei, D. M. Newns, C. C. Chi, and P. C. Pattnaik, Phys. Rev. Lett. **65**, 2724 (1990).
- [4] R. S. Markiewicz, J. Phys. Chem. Solids **58**, 1179 (1997).
- [5] C. Liu, T. Kondo, R. M. Fernandes, A. D. Palczewski, E. D. Mun, N. Ni, A. N. Thaler, A. Bostwick, E. Rotenberg, J. Schmalian, S. L. Bud'ko, P. C. Canfield, and A. Kaminski, Nat. Phys. **6**, 419 (2010).
- [6] Y. Quan and W. E. Pickett, Phys. Rev. B **93**, 104526 (2016).
- [7] J. L. Sarrao and J. D. Thompson, J. Phys. Soc. Jpn. **76**, 051013 (2007).
- [8] E. E. Rodriguez, D. A. Sokolov, C. Stock, M. A. Green, O. Sobolev, J. A. Rodriguez-Rivera, H. Cao, and A. Daoud-Aladine, Phys. Rev. B **88**, 165110 (2013).
- [9] R. Hlubina, Phys. Rev. B **53**, 11344 (1996).
- [10] A. A. Varlamov, V. S. Egorov, and A. Pantsulaya, Adv. Phys. **38**, 469 (1989).
- [11] E. A. Yelland, J. M. Barraclough, W. Wang, K. V. Kamenev, and A. D. Huxley, Nat. Phys. **7**, 890 (2011).
- [12] H. Pfau, R. Daou, S. Lausberg, H. R. Naren, M. Brando, S. Friedemann, S. Wirth, T. Westerkamp, U. Stockert, P. Gegenwart, C. Krellner, C. Geibel, G. Zwirgagl, and F. Steglich, Phys. Rev. Lett. **110**, 256403 (2013).
- [13] D. Aoki, G. Seyfarth, A. Pourret, A. Gourgout, A. McCollam, J. A. N. Bruin, Y. Krupko, and I. Sheikin, Phys. Rev. Lett. **116**, 037202 (2016).
- [14] G. Bastien, A. Gourgout, D. Aoki, A. Pourret, I. Sheikin, G. Seyfarth, J. Flouquet, and G. Knebel, Phys. Rev. Lett. **117**, 206401 (2016).
- [15] D. S. Grachtrup, N. Steinki, S. Süllow, Z. Cakir, G. Zwirgagl, Y. Krupko, I. Sheikin, M. Jaime, and J. A. Mydosh, Phys. Rev. B **95**, 134422 (2017).
- [16] H. Pfau, R. Daou, S. Friedemann, S. Karbassi, S. Ghanadzhadeh, R. Kuechler, S. Hamann, A. Steppke, D. Sun, M. Koenig, A. P. Mackenzie, K. Kliemt, C. Krellner, and M. Brando, arXiv:1612.06273.
- [17] B. Burganov, C. Adamo, A. Mulder, M. Uchida, P. D. C. King, J. W. Harter, D. E. Shai, A. S. Gibbs, A. P. Mackenzie, R. Uecker, M. Bruetzam, M. R. Beasley, C. J. Fennie, D. G. Schlom, and K. M. Shen, Phys. Rev. Lett. **116**, 197003 (2016).
- [18] See Supplemental Material at [URL here] for additional experimental data, further details of the experimental technique, and a description of the tight-binding simulations.
- [19] C. W. Chu, T. F. Smith, and W. E. Gardner, Phys. Rev. B **1**, 214 (1970).
- [20] D. R. Overcash, T. Davis, J. W. Cook, and M. J. Skove, Phys. Rev. Lett. **46**, 287 (1981).
- [21] C. L. Watlington, J. W. Cook, and M. J. Skove, Phys. Rev. B **15**, 1370 (1977).
- [22] C. W. Hicks, M. E. Barber, S. D. Edkins, D. O. Brodsky, and A. P. Mackenzie, Rev. Sci. Instrum. **85**, 065003 (2014).
- [23] C. W. Hicks, D. O. Brodsky, E. A. Yelland, A. S. Gibbs, J. A. N. Bruin, M. E. Barber, S. D. Edkins, K. Nishimura, S. Yonezawa, Y. Maeno, and A. P. Mackenzie, Science **344**, 283 (2014).
- [24] Y. Maeno, H. Hashimoto, K. Yoshida, S. Nishizaki, T. Fujita, J. G. Bednorz, and F. Lichtenberg, Nature **372**, 532 (1994).
- [25] A. P. Mackenzie and Y. Maeno, Rev. Mod. Phys. **75**, 657 (2003).
- [26] Y. Maeno, S. Kittaka, T. Nomura, S. Yonezawa, and K. Ishida, J. Phys. Soc. Jpn. **81**, 011009 (2012).
- [27] C. Kallin, Rep. Prog. Phys. **75**, 042501 (2012).
- [28] A. P. Mackenzie, T. Scaffidi, C. W. Hicks, and Y. Maeno, npj Quantum Mater. **2**, 40 (2017).
- [29] A. Steppke, L. Zhao, M. E. Barber, T. Scaffidi, F. Jerzembeck, H. Rosner, A. S. Gibbs, Y. Maeno, S. H. Simon, A. P. Mackenzie, and C. W. Hicks, Science **355**, eaaf9398 (2017).
- [30] Y.-C. Liu, F.-C. Zhang, T. M. Rice, and Q.-H. Wang, npj Quantum Mater. **2**, 12 (2017).
- [31] C. Bergemann, A. P. Mackenzie, S. R. Julian, D. Forsythe, and E. Ohmichi, Adv. Phys. **52**, 639 (2003).
- [32] D. O. Brodsky, M. E. Barber, J. A. N. Bruin, R. A. Borzi, S. A. Grigera, R. S. Perry, A. P. Mackenzie, and C. W. Hicks, Sci. Adv. **3**, e1501804 (2017).
- [33] M. E. Barber, Ph.D. thesis, University of St Andrews (2017).
- [34] A. P. Mackenzie, R. K. W. Haselwimmer, A. W. Tyler, G. G. Lonzarich, Y. Mori, S. Nishizaki, and Y. Maeno, Phys. Rev. Lett. **80**, 161 (1998).
- [35] Y. Maeno, K. Yoshida, H. Hashimoto, S. Nishizaki, S.-I. Ikeda, M. Nohara, T. Fujita, A. P. Mackenzie, N. E. Hussey, J. G. Bednorz, and F. Lichtenberg, J. Phys. Soc. Jpn. **66**, 1405 (1997).
- [36] N. E. Hussey, A. P. Mackenzie, J. R. Cooper, Y. Maeno, S. Nishizaki, and T. Fujita, Phys. Rev. B **57**, 5505 (1998).
- [37] N. Kikugawa, C. Bergemann, A. P. Mackenzie, and Y. Maeno, Phys. Rev. B **70**, 134520 (2004).
- [38] K. M. Shen, N. Kikugawa, C. Bergemann, L. Balicas, F. Baumberger, W. Meevasana, N. J. C. Ingle, Y. Maeno, Z.-X. Shen, and A. P. Mackenzie, Phys. Rev. Lett. **99**, 187001 (2007).
- [39] J. M. Buhmann, Phys. Rev. B **88**, 245128 (2013).
- [40] J. M. Buhmann, Ph.D. thesis, ETH Zurich (2013).
- [41] J. A. N. Bruin, H. Sakai, R. S. Perry, and A. P. Mackenzie, Science **339**, 804 (2013).
- [42] J. Paglione, C. Lupien, W. A. MacFarlane, J. M. Perz, L. Taillefer, Z. Q. Mao, and Y. Maeno, Phys. Rev. B **65**, 220506 (2002).

# Supplemental Materials for: Resistivity in the Vicinity of a Van Hove Singularity: $\text{Sr}_2\text{RuO}_4$ Under Uniaxial Pressure

M. E. Barber,<sup>1,2</sup> A. S. Gibbs,<sup>1</sup> Y. Maeno,<sup>3</sup> A. P. Mackenzie,<sup>1,2</sup> and C. W. Hicks<sup>2</sup>

<sup>1</sup> *Scottish Universities Physics Alliance, School of Physics and Astronomy,  
University of St. Andrews, St. Andrews KY16 9SS, U.K.*

<sup>2</sup> *Max Planck Institute for Chemical Physics of Solids, Nöthnitzer Str. 40, 01187 Dresden, Germany*

<sup>3</sup> *Department of Physics, Graduate School of Science, Kyoto University, Kyoto 606-8502, Japan*

## I. DETAILS OF THE EXPERIMENTAL TECHNIQUE

The piezoelectric based uniaxial pressure device used in this work was first described in [22, 23] and the later modifications in [29, 32, 33]. For this technique the samples are first prepared as long thin bars using a wire lapping saw and mechanical polishing. The sample is secured into the device using epoxy, holding the sample only by its ends and spanning across an adjustable gap in the device. When the two ends of the sample are pushed closer together or further apart to compress or tension the sample respectively, the central portion of the sample, where we measure its resistivity and susceptibility, is free to expand or contract as governed by the sample's Poisson's ratio. This means the stress, or equivalently the pressure, in the region of the sample where we measure is uniaxial but not the strain. However, we have better knowledge of the applied displacement and therefore the strain along the pressure axis. We measure the displacement applied between the two ends of the sample using a parallel plate capacitor, in line with, and beneath the sample. To calculate the strain we need to know the length of sample this displacement is applied to. This is not trivial and leads to the largest uncertainty in calculating the strain in the sample. Because the sample is held to the device using an epoxy which is relatively soft, the strained length of the sample is not the exposed length of sample between the two mounts, rather some of the epoxy in the mounts deforms too and the strained length is slightly longer. Exactly how much longer depends on the sample and epoxy geometry, and their elastic constants. We estimate the strained length using finite element simulations, the results of which and the relevant dimensions of the samples are presented in table S1. We used the elastic constants of  $\text{Sr}_2\text{RuO}_4$  from [42] and estimate the shear modulus of the epoxy, Stycast 2850FT, to be 6 GPa [22]. Because of the uncertainties in some of these values, all strains quoted have an uncertainty of  $\sim 20\%$  (a systematic error affecting all measured strains equally).

TABLE S1. Relevant sample and epoxy dimensions for calculating the strain transmission to the sample through the epoxy.  $w$  and  $t$  are the width and thickness of the sample.  $L_{\text{gap}}$  is the gap between the sample plates, the exposed length of sample.  $d_{\text{epoxy}}$  is the depth of epoxy above and below the sample joining to the sample plates.  $L_{\text{eff}}$  is the calculated effective length of the sample as described in the text.  $\varepsilon_{xx, \text{peak } T_c}$  is the strain at which the peak in  $T_c$  was observed for each sample.

sample number	growth	$w$ ( $\mu\text{m}$ )	$t$ ( $\mu\text{m}$ )	$L_{\text{gap}}$ ( $\mu\text{m}$ )	$d_{\text{epoxy}}$ ( $\mu\text{m}$ )	$L_{\text{eff}}$ ( $\mu\text{m}$ )	$\varepsilon_{xx, \text{peak } T_c}$ (%)
1	C362	320	90	1100	$\approx 25$	1510	-0.56
2	A1	310	100	1000	$\approx 25$	1430	-0.59

The samples used in this study come from two different batches. Each was prepared with six electrical contacts using the standard recipe, DuPont 6838 silver paste baked at  $450^\circ\text{C}$  for 5 minutes, before they were mounted into the pressure device. After mounting, two concentric coils were lowered above the sample to measure the diamagnetic signal of superconductivity by measuring the change in mutual inductance between the coils.

## II. ADDITIONAL DATA

The resistivity data for sample 1 are shown in the main text. The data for sample 2 are shown in Fig. S1. Note that the difference in strain scale is most probably not an intrinsic sample-to-sample variation, and rather comes from the experimental uncertainty in measuring the applied strain.

Additionally in Fig. S1, the strain dependence of the fitted residual resistivity is shown explicitly for both samples. To generate the temperature exponent colour maps in Figs. 4(a) and S1(d) the residual resistivity must be subtracted from the data before differentiating. To extrapolate below  $T_c$  a fit of the form  $\rho = \rho_{\text{res}} + BT^\delta$  was used and the range of the fit was chosen self consistently so that an approximately constant exponent is obtained over the temperature

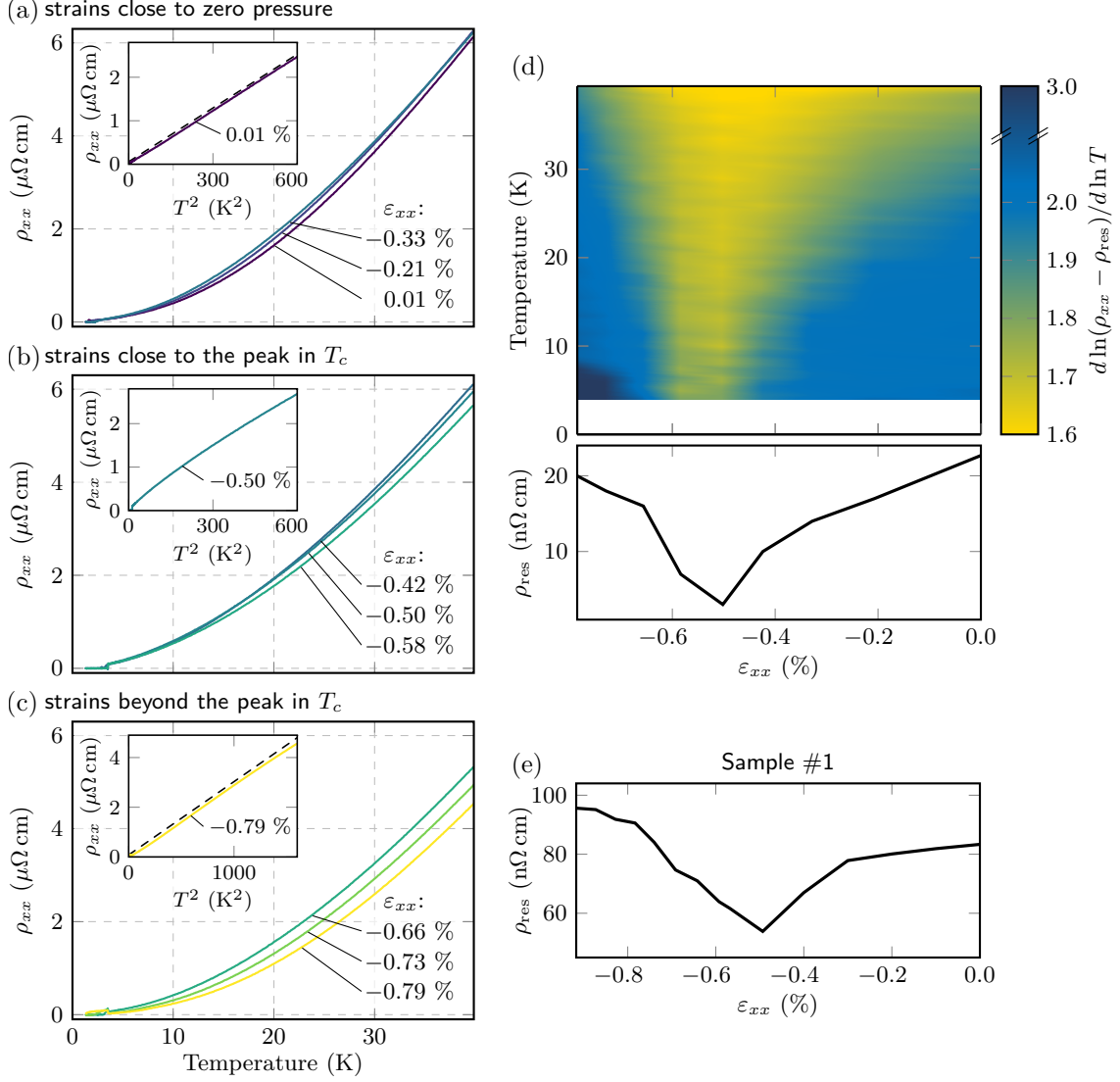


FIG. S1. Additional resistivity data. Panels (a), (b), and (c) show the resistivity temperature dependence of the second sample in the same three regions across the phase diagram as described in Fig. 3. Panel (d) shows the logarithmic derivative plot for the second sample, depicting the resistivity temperature exponent  $\delta$  as calculated in Fig. 4, and the residual resistivity used for extracting the exponent. Panel (e) shows the residual resistivity of sample 1 used to generate Fig. 4 in the main text.

range of the fit. Although the exact position of the crossover from  $T^2$  to a lower power is slightly sensitive to the details of this fitting the overall picture is unchanged. Similarly, although the fitted residual resistivity has a weak strain dependence if left as a free parameter, it is so small for both these samples that fixing it to be strain-independent makes no qualitative difference to the logarithmic derivative plots or the value of  $\delta$  deduced for  $\varepsilon_{xx} \sim -0.5$  %.

Fig. 4 in the main text compares two curves of the strain dependence of  $T_c$  with the resistivity at 4.5 K.  $T_c$  was obtained from temperature dependent a.c. magnetic susceptibility  $\chi'(T)$  measurements and taken to be the midpoint of the transition. Fig. S2 shows the susceptibility measurements for both samples at a variety of strains.

### III. DETAILS OF THE TIGHT BINDING SIMULATIONS

Fig. 1 in the main text presents an illustrative tight-binding simulation of the different effects of biaxial and uniaxial pressure. We start from the simplest 2D nearest and next-nearest neighbour tight-binding model

$$\Delta E(\mathbf{k}) = -2t[\cos(k_x a) + \cos(k_y b)] - 2t'[\cos(k_x a + k_y b) + \cos(k_x a - k_y b)], \quad (\text{S1})$$



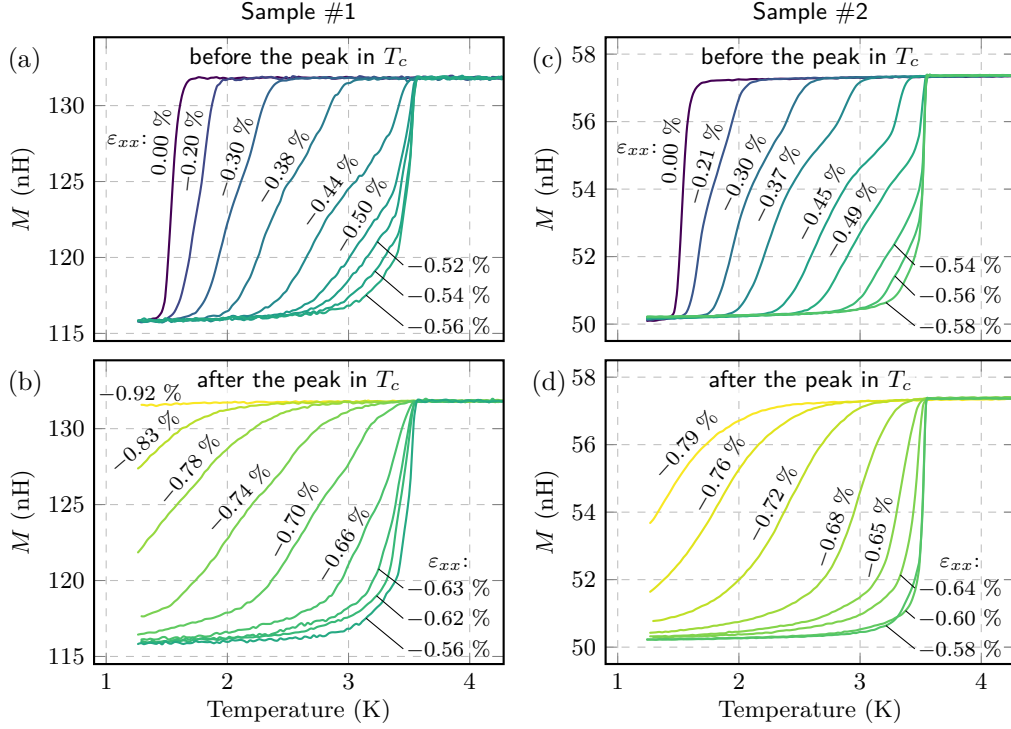


FIG. S2. A.c. magnetic susceptibility measurements of both samples at various strains  $\varepsilon_{xx}$  used for identifying  $T_c(\varepsilon_{xx})$ . (a) and (c) show measurements below the peak in  $T_c$  for samples 1 and 2 respectively, (b) and (d) show measurements above the peak in  $T_c$ .  $M$  is the mutual inductance between the two coils of the susceptibility sensor.

where  $a$  and  $b$  are the lattice constants in the  $x$  and  $y$  directions. We set the ratio  $t'/t = 0.3$  and work at half filling.

Under biaxial pressure, changes in the Fermi surface shape can only occur if the ratio of  $t'/t$  changes. Generally it is expected that  $t'$  will increase faster than  $t$  under compression [17]. For our simulations we make the simplest assumption that the hoppings depend linearly on lattice strain and make the next-nearest neighbour hopping increase 20 % faster with strain than the nearest neighbour hopping. Biaxial pressure causes the unit cell lattice vector  $a$  to change as

$$a(\varepsilon) = b(\varepsilon) = a_0(1 + \varepsilon), \quad \varepsilon = \frac{1 - \nu_{xy}}{E} \sigma, \quad (\text{S2})$$

where  $\sigma$  is the applied stress and the resultant strain  $\varepsilon$  depends on the Young's modulus  $E$  and Poisson's ratio  $\nu_{xy}$ . We set the strain dependence of the hopping terms to

$$t(\varepsilon) = t_0(1 - \alpha\varepsilon) \quad t'(\varepsilon) = t'_0(1 - 1.2\alpha\varepsilon). \quad (\text{S3})$$

where  $\alpha$  is an adjustable parameter that scales the effect of strain.

Equal uniaxial pressures cause much larger changes to the Fermi surface due to the much larger distortion of the unit cell as it is able to relax orthogonal to the pressure axis according to Poisson's ratio. For the simulation we keep the same starting parameters as the biaxial simulation but now allow the hoppings to change anisotropically. The unit cell deforms as

$$a(\varepsilon) = a_0(1 + \varepsilon_{xx}), \quad b(\varepsilon) = a_0(1 - \nu_{xy}\varepsilon_{xx}), \quad \varepsilon_{xx} = \sigma_{xx}/E, \quad (\text{S4})$$

and the hoppings are now different along the  $x$  and  $y$  directions

$$t_x(\varepsilon) = t_0(1 - \alpha\varepsilon_{xx}), \quad t_y(\varepsilon) = t_0(1 + \alpha\nu_{xy}\varepsilon_{xx}), \quad t'(\varepsilon) = t'_0(1 - \alpha(1 - \nu_{xy})\varepsilon_{xx}/2). \quad (\text{S5})$$

In the case for  $\text{Sr}_2\text{RuO}_4$ , Fig. 2 in the main text, we start from the tight-binding parametrisation derived from fits to experimental data [31] which sets the ratios of each of the hoppings, but rather than using DFT calculations to set the magnitude we use the mass renormalisation from [38]. We use the measured Poisson's ratio of 0.39 [42] and scale the hopping strengths in the same manner as for the uniaxial case above while keeping the total electron count constant.